Journal of Rheology

RESEARCH ARTICLE | FEBRUARY 02 2024

Creep and recovery in dense suspensions of smooth and rough colloids

Yug Chandra Saraswat ; Eli Kerstein ; Lilian C. Hsiao

J. Rheol. 68, 205–217 (2024)
https://doi.org/10.1122/8.0000722

Creep and recovery in dense suspensions of smooth and rough colloids

Yug Chandra Saraswat, Eli Kerstein, and Lilian C. Hsiao[a)]

Department of Chemical and Biomolecular Engineering, North Carolina State University, Raleigh, North Carolina 27695

(Received 5 July 2023; final revision received 27 December 2023; published 2 February 2024)

Abstract

We report the effect of particle surface roughness on creep deformation and subsequent strain recovery in dense colloidal suspensions. The suspensions are composed of hard-spherelike poly(methyl methacrylate) smooth (S) and rough (R) colloids with particle volume fractions $\phi^S = 0.64 \pm 0.01$ and $\phi^R = 0.56 \pm 0.01$, corresponding to a distance of 3.0% and 3.4% based on their jamming volume fractions ($\phi_J^S = 0.66 \pm 0.01$, $\phi_J^R = 0.58 \pm 0.01$). The suspensions are subject to a range of shear stresses (0.01–0.07 Pa) above and below the yield stress values of the two suspensions ($\sigma_y^S = 0.035$ Pa, $\sigma_y^R = 0.02$ Pa). During creep, suspensions of rough colloids exhibit four to five times higher strain deformation compared to smooth colloids, irrespective of the applied stress. The interlocking of surface asperities in rough colloids is likely to generate a heterogeneous microstructure, favoring dynamic particle activity and percolation of strain heterogeneities, therefore resulting in higher magnitude of strain deformation and an earlier onset of steady flow. Strain recovery after the cessation of stress reveals a nonmonotonic recoverable strain for rough colloids, where the peak recoverable strain is observed near the yield stress, followed by a steep decline with increasing stress. This type of response suggests that frictional constraints between geometrically frustrated interlocking contacts can serve as particle bonds capable of higher elastic recovery but only near the yield stress. Understanding how particle roughness affects macroscopic creep and recovery is useful in designing yield stress fluids for additive manufacturing and product formulations.
 https://doi.org/10.1122/8.0000722

I. INTRODUCTION

Yield stress fluids belong to a class of materials that exhibit solidlike response below a certain bulk stress and liquidlike response at larger applied stresses. The critical stress that characterizes this transition is called the yield stress [1]. Dense colloidal suspensions that exhibit yield stress behavior are found in applications such as consumer and pharmaceutical formulations [2,3], oil and gas recovery [4], additive manufacturing [5,6], controlled drug delivery [7,8], and flow batteries for energy storage [9]. In these cases, the yield stress and flowability of formulations are achieved by tuning the properties of constituent units [10,11]. Particle properties such as stiffness [12,13], shape [5,6,14], polydispersity [15,16], and interparticle interactions [17–20] have been shown to strongly affect the yielding transition. However, studies that examine the effects of particle surface roughness on the yielding of colloidal suspensions are lacking.

Colloidal particles with corrugated surfaces and asperities often experience hindered rotational dynamics in dense suspensions near the jamming point. Smaller colloids and nanoparticles with a greater degree of thermal fluctuations are less susceptible, but particles with asperity heights exceeding the thickness of steric brush layers are particularly prone to such types of frictional constraints [21,22], which arise due to frustration caused by the interlocking of surface asperities in near contact [23]. The roughness-induced frictional constraints cause changes in the solvent hydrodynamics between interstitial spaces and in the linear viscoelastic response of the suspension. Pradeep *et al.* showed that the hydrodynamic interactions in sterically stabilized rough colloids transition between a freely draining system to a fully lubricated state when the volume fraction increases, while Schroyen *et al.* found similar behavior for hairy and rough silica colloids sheared at high frequencies [24,25]. Ilhan *et al.* found that surface roughness causes a second colloidal glass transition to develop at high particle concentrations where the surface-to-surface separation is equivalent to the particle roughness length scale [26]. The roughness-induced second glass transition is characterized by highly suppressed and subdiffusive rotational dynamics.

The hindered rotational dynamics of rough particles significantly change the rheology of colloidal suspensions, such as causing the early onset of shear thickening at low stresses [27–32], enhancing the stability of Pickering emulsions [33–37], causing jamming in constricted particulate flows [38], and increasing the bond rigidity in fractal colloidal gel networks [39]. Here, we focus on the creep and recovery of dense colloidal suspensions composed of surface-isotropic (smooth, S) and surface-anisotropic (rough, R) particles with hard-spherelike behavior (volume fractions, $\phi^S = 0.64 \pm 0.01$, $\phi^R = 0.56 \pm 0.01$) at 3% distance from jamming (jamming volume fractions, $\phi_J^S = 0.66 \pm 0.01$, $\phi_J^R = 0.58 \pm 0.01$). The reason for choosing suspensions near the jamming transition is because the interparticle surface separation is minimized, which maximizes the influence of surface roughness on the macroscopic flow behavior. Since smooth and rough

a)Author to whom correspondence should be addressed; electronic mail: lilian_hsiao@ncsu.edu

colloids jam at different volume fractions, the parameter known as the distance from jamming is used throughout this work as the basis of comparison for the rheological responses. Earlier studies have shown that the distance from jamming is a strong predictor of shear thickening in dense colloidal suspensions [27]. Similar parameters based on the distance from maximum packing have been found to correlate well with the yield stress and elasticity of suspensions composed of shape-anisotropic colloids [5,14]. At moderate to high volume fractions (i.e., short distance from jamming), colloids become trapped in a nonequilibrium glassy state where the particle dynamics are strongly influenced by near-field and far-field crowding effects. Each particle is trapped by its neighbors in correlated clusters or so-called cages and, therefore, must cooperate with its neighboring particles to move a certain distance [40–43]. At short times, the particle mobility is limited by the cage size (β-relaxation), while at longer times, the cages relax (α-relaxation) and allow particles to diffuse beyond their first coordination shell. At very high volume fractions and very close to jamming, the system is trapped in a frustrated glasslike state where the α-relaxation is nearly absent [44].

Shear-induced yielding in colloidal glasses and dense suspensions has been the subject of intense research [41,45–53], where the link between the microstructure, dynamics, and rheology is established through techniques such as confocal microscopy [50,54–56], scattering [51,57–59], and micro-rheological tools such as optical tweezers [60]. These results collectively demonstrate a strong correlation between clusters of dynamically active particles and the onset of macroscopic fluidization. Petekidis *et al*. used creep and recovery rheology to systematically investigate shear-induced deformation in hard-sphere colloidal glasses above and below the yield stress [45–48]. Below the yield stress, strain deformation during creep and strain recovery upon cessation of shear is dependent on the solidlike elastic behavior of the suspension, indicated by a linear increase in strain and recoverable strain with an increasing applied stress. Above the yield stress, steady viscous flow is observed during creep while the magnitude of strain recovery reaches a saturated value. The significant strain recovery above the yield stress is attributed to the elastic distortion of particle cages or the so-called cage elasticity. The yielding behavior of glassy materials has been modeled using mode coupling theory [61–63], which computes the probability of a particle to overcome the entropic barrier required to move beyond its cage. The barrier height and diffusion length scale are important contributors to particle dynamics in this model [64–66]. Mean-field theories have also been applied to shape-anisotropic particles such as uniaxial dicolloids to model the presence of multiple glassy states and distinct yielding events associated with overcoming rotational and translational constraints [5,6,14,67,68]. As mentioned earlier, the existence of multiple glassy states has been experimentally observed for raspberry-shaped colloidal particles due to suppression of the translational and rotational motion at different volume fractions [26]. Because rough colloids in jammed suspensions exhibit both rotational and translational constraints, they are expected to display yielding and strain recovery behavior that is distinct from that of smooth colloids.

In this work, we use creep and recovery experiments to study the response of smooth and rough colloids above and below the bulk yield stress of the suspensions (applied stress range, $\sigma = 0.01$–0.07 Pa). Compared to smooth colloids, jammed suspensions of rough colloids exhibit a lower load-bearing capacity within the linear viscoelastic regime (LVR) and higher strain deformation above and below the yield stress. When recovering from the applied creep stress, rough colloids show higher total recoverable strain compared to smooth colloids. Furthermore, the total recoverable strain in rough colloids changes nonmonotonically with respect to the applied stress, a trend previously seen in attractive colloidal glasses [17,69,70]. The results suggest that there is a higher elastic recovery of interlocked rough particle clusters when suspensions are sheared near the yield stress of 0.02 Pa due to frictional constraints between neighboring particles [21,22].

II. EXPERIMENTAL SECTION

A. Materials

All chemicals were purchased from Sigma Aldrich. Methyl methacrylate (MMA, 99%) and ethylene glycol dimethylacrylate (EGDMA, 98%) were purified using an inhibitor removal column and stored in a refrigerator at 4 °C. Azo-bis-isobutyronitrile (AIBN) was recrystallized in acetone. 1-Octanethiol (≥98.5%), methacrylic acid (MA, 99%), hexane (≥97%), dodecane (99%), and squalene (98%) were used without further purification. The poly(12-hydroxystearic acid)-(glycidyl methacrylate)-(methyl methacrylate) (PHSA-GMA-MMA) block copolymer was synthesized in the laboratory using a method described previously by Pradeep *et al*. [71].

B. Particle synthesis and characterization

Sterically stabilized smooth and rough poly(methyl methacrylate) (PMMA) colloidal particles were synthesized using a free-radical dispersion polymerization technique [71]. Briefly, a solvent mixture containing 7.5 g of hexane, 2.5 g of dodecane, and 1.2 g of PHSA was heated in a round bottom flask at 80 °C. Once the mixture was heated, 10 g MMA, 200 µl MA, 75 µl 1-octanethiol, and 8.5 mg of AIBN were added to the flask. The nucleation and oligomer precipitation process began in 4–6 min, which resulted in a turbid reactant solution. The reaction was allowed to proceed for 2 h. Figure 1(a) shows the resultant synthesis of PHSA-PMMA colloids with smooth surfaces and spherical morphology. To introduce surface roughness, an additional step involving the dropwise addition of cross-linking agent, EGDMA, was performed at the onset of nucleation. The cross-linking agent likely causes microphase separation of the precipitated oligomers and provides additional sites for randomized growth [22], leading to the formation of rough colloids as shown in Fig. 1(b). All particles were dyed using Nile Red to enable imaging using confocal laser scanning microscopy (Leica, SP8). Once the synthesis was complete,

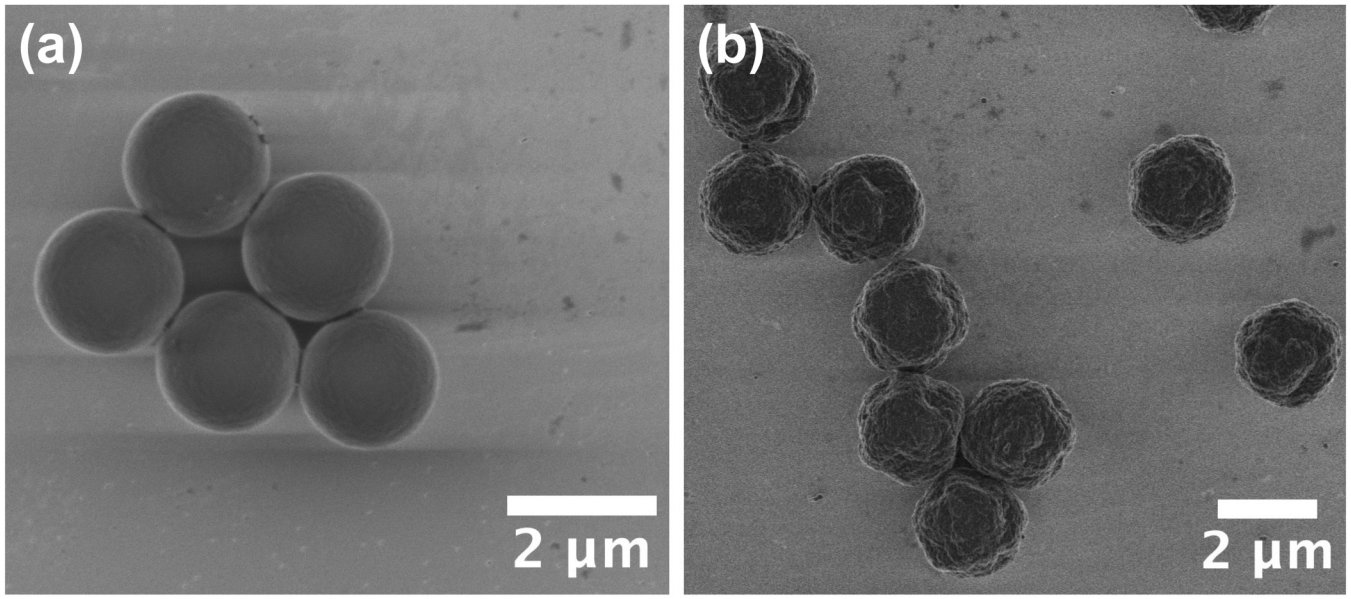

FIG. 1. Representative scanning electron micrographs of (a) smooth and (b) rough PHSA-PMMA colloids synthesized using free-radical polymerization.

the particles were cleaned with hexane five times by centrifugation at 10 000 rpm for 10 min and stored in an amber bottle until further use.

C. Preparation of dense suspensions

Dense suspensions of smooth and rough PMMA colloids in squalene exhibit different jammed packing fractions, $\phi_J^S = 0.66 \pm 0.01$ for smooth and $\phi_J^R = 0.58 \pm 0.01$ for rough colloids. The value of ϕ_J^S for smooth colloids is in agreement with simulations that account for size polydispersity [72–74]. The ϕ_J^R value for rough colloids is lower than that of smooth colloids likely due to hindered rotational dynamics from surface asperities as observed in previous studies [27,28]. Due to the differences in the jamming fractions of smooth and rough colloids, results are normalized using the distance from jamming $(\phi_J - \phi)/\phi_J$, which is 3.0% and 3.4% for smooth and rough colloids, respectively. All experiments were conducted as close to ϕ_J as possible to minimize surface-to-surface separation between particles, which maximizes the influence of surface roughness on suspension rheology.

The particles are charge neutral and refractive index-matched in this solvent, which effectively suppresses any electrostatic interactions and van der Waals attractions and ensures hard-spherelike interactions between the particles [71]. Hard-sphere interactions between particles are verified by ensuring a good fit between measured the experimentally measured radial distribution functions $g(r)$ and the hard-sphere Ornstein–Zernicke equation of state solved with the Percus–Yevick closure [75]. This was also demonstrated by Pradeep *et al.* for both smooth and rough colloids over a wide range of particle volume fractions [71]. The particles may undergo swelling in squalene due to polymer-solvent interactions. Rather than measuring the dry particle size using scanning electron microscopy, an effective diameter ($2a_{eff}$) was obtained from 2D confocal microscopy images of colloidal suspensions near the coverslip, where particles form a monolayer. The effective particle diameters and the associated size polydispersity for smooth and rough colloids suspended in squalene were $2a_{eff} = 2.21\,\mu\text{m} \pm 3\%$ and $= 2.23\,\mu\text{m} \pm 4\%$. The effective particle diameters for both smooth and rough colloids were obtained by averaging surface-to-surface measurements of at least 50 particles obtained from imaging. The distribution of the particle diameter computed by dividing the standard deviation associated with the measured diameters by the mean diameter. The large number of measurements allowed us to minimize statistical uncertainty associated with particle sizes, especially with rough colloids. This technique was reported earlier in a previous publication [71]. A circularity parameter ($\psi_{2D} = (4A_p)/P_P^2$, where A_p is the projected area of particle in 2D and P_p is the particle perimeter) was used to quantify the morphological deviation of rough colloids from that of their spherical counterparts. The circularity values were $\psi_{2D} = 1.00 \pm 0.01$ for smooth colloids and $\psi_{2D} = 0.90 \pm 0.03$ for rough colloids.

After cleaning the particles and performing solvent transfers from hexane to squalene, dilute suspensions were centrifuged at high speeds until most of the particles had settled. Centrifugation was performed over 3 h at a gravitational Peclet number of $Pe_g = (4\pi\Delta\rho g a_{eff}^4)/3k_BT = 5000$, where k_B is the Boltzmann constant, T is the temperature, and $\Delta\rho$ is the density mismatch between the solvent and the particles ($\Delta\rho = 0.322\ \text{g/cm}^3$). The centrifugation step ensured the formation of disordered sediments at $\phi^S = 0.64 \pm 0.01$ and $\phi^R = 0.56 \pm 0.01$. After removing the excess solvent, the suspensions were placed on horizontal rollers for at least 5 days to fully redisperse. Confocal microscopy was used to obtain 3D image volumes of the suspensions. Particle centroids were identified for smooth and rough colloids, and the particle volume fraction ($\phi = (4\pi a_{eff}^3 N_P)/3V_{box}$) was obtained by measuring the number of particle centroids (N_P) within the imaging volume, V_{box} [71]. We computed the distance from

jamming for smooth and rough colloids by fitting Eilers' model $[\eta_{r\infty} = (1 + 1.5\phi(1 - \phi/\phi_J)^{-1}))^2]$ to the high shear relative viscosity ($\eta_{r\infty}$) as a function of ϕ [76]. Figure 2 shows Eilers' fit to the relative viscosity as a function of volume fraction for smooth and rough colloids.

D. Preshear and rheological protocol

All rheological experiments were conducted on a stress-controlled rheometer (TA Instruments, DHR-2) at 20 °C using a 50 mm parallel plate geometry. The diameter of the parallel plate geometry was chosen to ensure that the torque signal, even at the lowest applied stress ($\sigma = 0.01$ Pa, torque = 245 nN m), was well above the DHR-2 rheometer's minimum torque limit (10 nN m). To prevent deformation due to residual torques during the recovery measurements, we performed rotational mapping before every experiment. The residual torque was of the order of ±14 nN m measured by performing a peak hold test at 0.1 rad/s for 120 s without loading the sample as recommended by the manufacturer. Since the applied torque signal, even at the lowest stress ($\sigma = 0.01$ Pa, torque = 245 nN m), is an order of magnitude above the measured residual torque, it is safe to assume that the strain responses during recovery were reliable. Furthermore, we used an inertial braking technique known as creep braking to eliminate the momentum of the rotating shaft during recovery. This technique compensates for the kinetic energy stored in the rotating top geometry by applying a reactive torque in the opposite direction within 10–15 ms.

A fixed gap height of 500 μm was chosen to avoid flow confinement effects. The top plate was slowly lowered onto the sample and the axial force was allowed to equilibrate around $F_N = (0 \pm 0.1)$ N, which significantly reduced normal stress effects on the shear rheology. To minimize wall slip, which can strongly influence creep and recovery experiments in colloidal glasses, sandpaper (1500 grit, $Ra = 1.76 \pm 0.46$ μm) was adhered to the top and bottom geometries [77,78]. The arithmetic mean roughness of the sandpaper was obtained using a confocal laser scanning microscope that uses interferometry to measure surface profiles (Keyence VKx1100). The optimum surface roughness for suppressing slip in nonaggregating particle suspensions is equivalent to that of the particle size [79,80]. In our system, $Ra \sim 2a_{eff}$ for both smooth and rough colloids. A common observation associated with the presence of wall slip is the dependence of rheological data on gap height [81,82]. Figure 3 confirms the absence of wall slip by showing that the error associated with the mean of time-dependent moduli of suspensions of smooth colloids obtained at three different gap heights is insignificant.

An oscillatory stress sweep was performed to identify the LVR, shear thinning, and the strain stiffening regime for all colloidal suspensions tested in this study. Figure 4 shows that the LVR for both types of suspensions exists up to 0.01 Pa, followed by a shear thinning regime up to 0.1 Pa for rough colloids and 1 Pa for smooth colloids. Higher applied stresses result in strain stiffening. The onset of strain stiffening for rough colloids occurs at lower stresses than that of smooth colloids because of the interlocking of surface asperities and formation of load-bearing force chains [27,28]. A stepwise growth is observed in suspensions of smooth and rough colloids within the strain stiffening regime similar to a two-step shear thinning to thickening transition, indicating order-disorder transitions previously reported for monodisperse colloidal suspensions with low yield stress and high loss tangent [83].

We note that all creep experiments were performed in the LVR and shear thinning regime ($\sigma = 0.01$ Pa–0.07 Pa, $\sigma a_{eff}^3/k_BT = 2.5 - 24$) but not within the strain stiffening regime to avoid dilatancy effects.

Preshear protocols are important in the study of out-of-equilibrium glassy suspensions because sample loading and stress history can strongly affect the measured rheological properties [84,85]. Figure 5 is a schematic

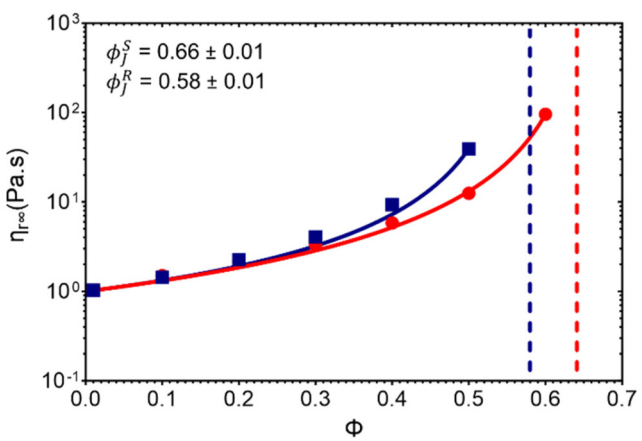

FIG. 2. Relative high shear steady viscosity as a function of particle volume fraction for suspensions of smooth (red circles) and rough colloids (blue squares). Continuous curves represent Eilers' fit. The vertical dashed lines represent jamming volume fractions for smooth (red dashed line at volume fraction = 0.66) and rough (blue dashed line at volume fraction = 0.58) colloids.

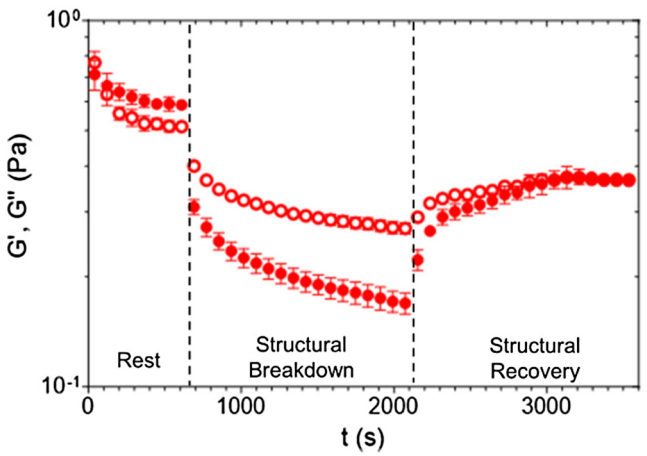

FIG. 3. The absence of wall slip verified by plotting mean and associated error in storage (closed symbols) and loss moduli (open symbols) measured at three different gap heights of 340, 600, and 770 μm during preshear for suspensions of smooth colloids ($2a_{eff} = 2.21 \pm 3\%$) at a distance of 3.0% from jamming. Dashed lines indicate transitions from the resting state (0.005 Pa) to structural breakdown at 0.05 Pa and structural recovery within the linear regime (0.005 Pa).

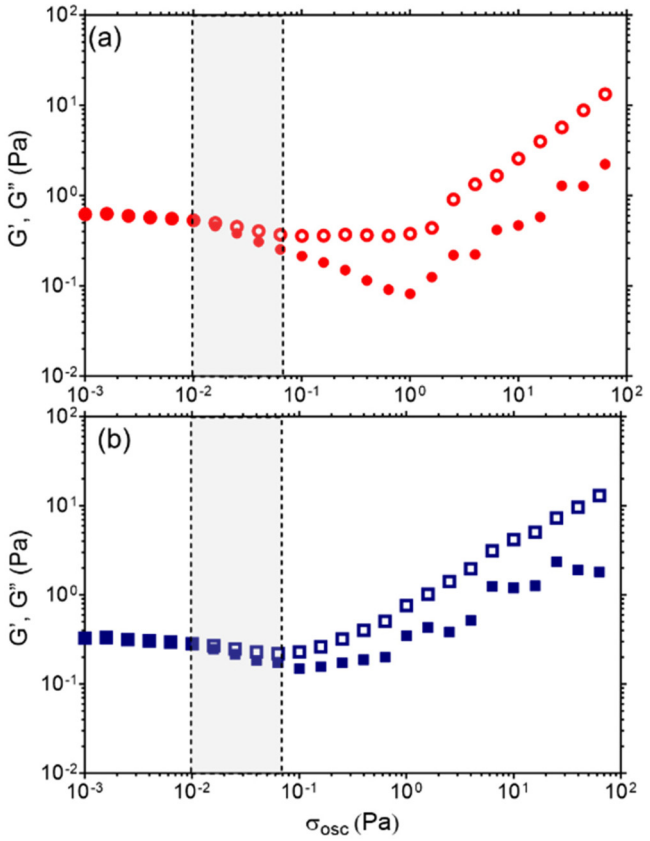

FIG. 4. Storage (closed symbols) and loss moduli (open symbols) obtained from oscillatory amplitude sweep showing the LVR, the onset of nonlinearity, and strain stiffening regime for (a) smooth (red circles) and (b) rough (blue squares) colloids at a distance of 3.0% and 3.4%, for smooth and rough colloids, respectively, from jammed packing. Regions within the dotted lines represent the range of applied stresses used in creep and recovery experiments.

representation of the preshear protocol that was applied to all samples in this study. The first step involved equilibrating the sample for 600 s under a small oscillatory stress of 0.005 Pa within the LVR, after which the suspension was rejuvenated at a high stress of 0.05 Pa in the nonlinear regime for 1500 s. The final step involved reducing the stress back to 0.005 Pa for 1500 s, during which the sample microstructure was allowed to recover to a steady and macroscopically reproducible state. Reproducibility is implied when the G' and G'' values obtained during the structural recovery do not vary by more than ±5% with time at the end of the recovery step, and the mean steady values of G' and G'' have an associated standard error of ±10% between different experiments for both smooth and rough colloids. All oscillatory preshear experiments were performed at a frequency of 0.3 rad/s.

After the preshear step, a constant stress ($0.01 \leq \sigma \leq 0.07$ Pa) was applied for 1000 s, followed by a zero-stress recovery step for 3000 s. During recovery, the recoverable strain was measured as a function of time. Suspensions of smooth and rough colloids were compared based on the total accumulated strain and rate of change in strain during creep. During recovery, the ability of the suspensions to recover the strain deformation was assessed based on the maximum recoverable strain at the end of the recovery step, and its ratio with respect to the maximum strain deformation at the end of creep. The creep and recovery experiments were performed in duplicates. All error bars indicate uncertainty associated with the mean values. Additionally, the yield stress values were verified by fitting the Herschel–Bulkley equation to steady shear flow sweeps between 0.01–1 Pa for smooth colloids and 0.01–0.1 Pa for rough colloids. At each applied stress, the shear rate was measured and averaged over a maximum equilibration time of 120 s. The measured shear rate at a given stress was reported if three consecutive measurements were within 5% of each other.

III. RESULTS AND DISCUSSION

A. Preshear rheology

Figure 6 shows that the preshear protocol ensures that each creep and recovery experiment begins with a reproducible initial state. The storage (G') and loss moduli (G'') remain constant up to 600 s after sample loading since the initial applied oscillatory stress ($\sigma = 0.005$ Pa, $\omega = 0.3$ rad/s) lies within the linear regime. After which, large stresses

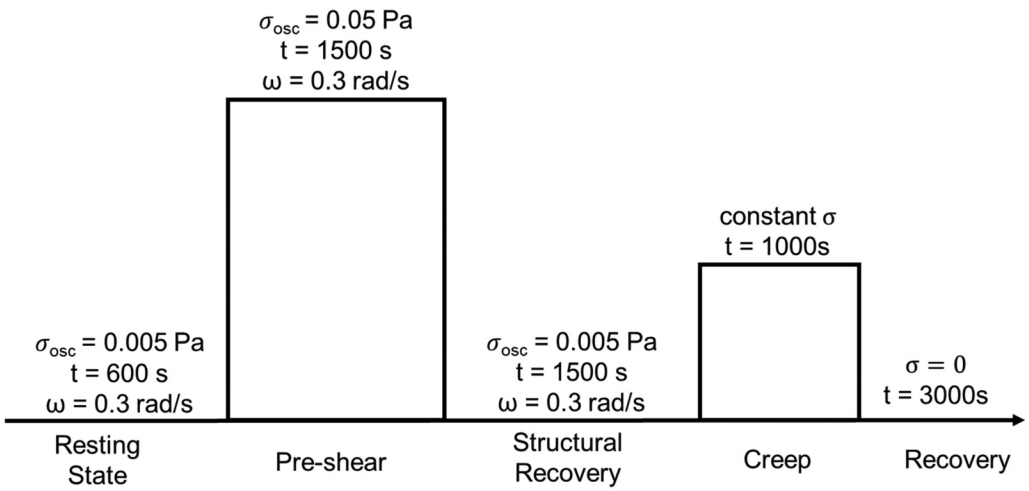

FIG. 5. Schematic representation of the preshear and subsequent creep and recovery protocol used in this study.

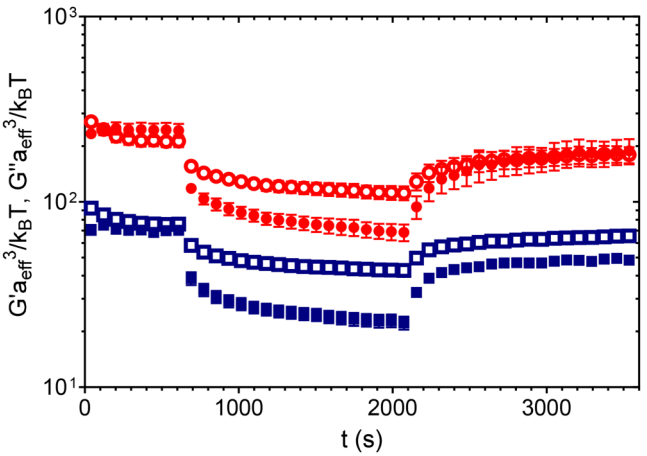

FIG. 6. Storage (closed symbols) and loss moduli (open symbols) scaled with respect to the particle size obtained from the preshear step showing the resting state after sample loading, the structural breakdown during preshear, and structural recovery during the waiting period for smooth (red circles) and rough (blue squares) colloids at a distance of 3.0% and 3.4%, for smooth and rough colloids, respectively, from jamming.

($\sigma = 0.05$ Pa, $\omega = 0.3$ rad/s) break the microstructure for 1500 s as indicated by the decreasing viscoelastic moduli of both systems. After 2200 s, the applied stress is again reduced ($\sigma = 0.005$ Pa, $\omega = 0.3$ rad/s), and the microstructure recovers to a steady and reproducible state at 3600 s. At the end of the structural recovery step, suspensions of rough colloids exhibit G' values that are approximately three times lower than that of suspensions of smooth colloids ($G'_R = 0.14 \pm 0.02$ Pa, $G'_S = 0.55 \pm 0.09$ Pa).

The differences in the storage moduli might be due to structural differences in the sample-spanning network of slow-moving particles that percolate throughout the sample. These slow clusters and networks have previously been shown to significantly contribute to the elasticity in a colloidal glass [86], and the effective cluster size could be larger for the rough colloids due to asperity interlocking. The shear rejuvenation step of the preshear protocol may not completely separate interlocked clusters of rough colloidal particles, resulting in a heterogeneous and weaker load-bearing microstructure. Since clusters have an effective size that is greater than the diameter of a single rough particle, and because the suspension stress scales as $1/a_{eff}^3$, the presence of larger and more heterogeneous clusters could reduce the elastic modulus [87,88]. Estimation of the cluster size based on the ratio of storage moduli for both systems, $(G'_S/G'_R)^{1/3} = (a_R/a_S)$, suggests that the radius of an interlocked cluster of rough colloids is 1.3 times that of the radius of a single smooth particle. Suspensions of smooth colloids may possess a more homogeneous microstructure after rejuvenation by avoiding cluster formation.

B. Creep

A large variety of flow responses that span shear rates corresponding to $0.01 < Pe < 14$ is observed in during creep. Here, $Pe = \dot{\gamma} a_{eff}^2/D(\phi)$ and $D(\phi) = 0.07D_0$, where D_0 is the translational diffusion coefficient for the dilute regime using the Stokes–Einstein–Sutherland equation. The prefactor 0.07 accounts for particle interactions near jammed packing [89], and $\dot{\gamma}$ is the shear rate measured during creep. At low Pe, slow creeping flows of glassy colloidal suspensions are dominated by thermal fluctuations and cage relaxation. Previous studies have shown that particle cages that form in quiescent colloidal glasses are generally isotropic [45,47]. However, an external shear stress applied during a creep experiment can cause an immediate elastic distortion of cages, resulting in instantaneous strain deformation ($t \sim 1$ s) followed by slow and continuous creep deformation at stresses below the yield stress ($\sigma < \sigma_y$) or steady flow above the yield stress ($\sigma \geq \sigma_y$) [52,90]. A simple way to analyze the creep response is by fitting a power law model $\gamma(t) = a\,t^b$, where γ represents strain deformation, a is the power law prefactor, and b indicates the rate of change in strain, to the strain deformation and tracking the change in the power law exponents over t. Creep flow is indicated by a continuous sublinear growth in strain ($b < 1$) with time, while a linear increase in strain ($b = 1$) represents completely viscous flow. The continuous sublinear growth observed at $\sigma \ll \sigma_y$ is often characterized by a power law exponent between 0.6 and 0.7. Such a response has been previously reported for metallic, polymer, and hard-sphere glasses [52,91,92].

Power law fits to the strain deformation curves over each decade in Figs. 7(a) and 7(b) indicate that suspensions of smooth and rough colloids yield and achieve steady flow above 0.035 and 0.020 Pa, respectively. Both suspensions exhibit an initial super-linear increase ($b = 1.2 \pm 0.1$) in strain between $0.1 < t < 1$ s, irrespective of the applied stress, which can be attributed to a competition between the rheometer inertia and sample elasticity [93]. At intermediate times ($1 < t < 10$ s), irrespective of the surface roughness, both suspensions show a constant sublinear increase with $b = 0.6 \pm 0.1$, suggesting that individual particles remain somewhat trapped within the cage formed by their neighboring particles [50]. At longer times ($10 < t < 1000$ s), there is a substantial deviation in the power law exponents with suspensions of smooth colloids displaying a gradual increase in the strain deformation ($b = 0.6 \pm 0.1$ for $0.01 \leq \sigma \leq 0.02$ Pa, $0.7 \leq b \leq 1.0$ for $0.035 \leq \sigma \leq 0.07$ Pa), while suspensions of rough colloids undergo a much more rapid deformation ($b = 0.6 \pm 0.1$ for $\sigma = 0.01$ Pa and $0.8 \leq b \leq 1.0$ for $0.02 \leq \sigma \leq 0.07$ Pa). Figures 7(c) and 7(d) represent the same result by replotting $\dot{\gamma}$ as a function of t. Once the suspensions yield and steady flow has been established, strain increases linearly with t and the shear rate remains constant as a function of time. On average, the slope of $\dot{\gamma}$ as a function of t is nearly zero over the last decade for $\sigma \geq 0.02$ Pa for suspensions of rough colloids and $\sigma > 0.035$ Pa for suspensions of smooth colloids.

Furthermore, a Herschel–Bulkley fit ($\sigma = \sigma_y + K\dot{\gamma}^n$) to the steady shear flow sweep curves, as shown in Fig. 8, results in $\sigma_y^S = 0.031$ Pa, $\sigma_y^R = 0.014$ Pa. The mean values of parameters K and n are 4.49 and 0.98 for smooth colloids and 1.33 and 1.01 for rough colloids, respectively. Based on the data collected from creep experiments, steady shear flow, and oscillatory stress sweep, we conclude that the yield stress values in suspensions of smooth and rough colloids at 3.0% and 3.4% distance from jamming

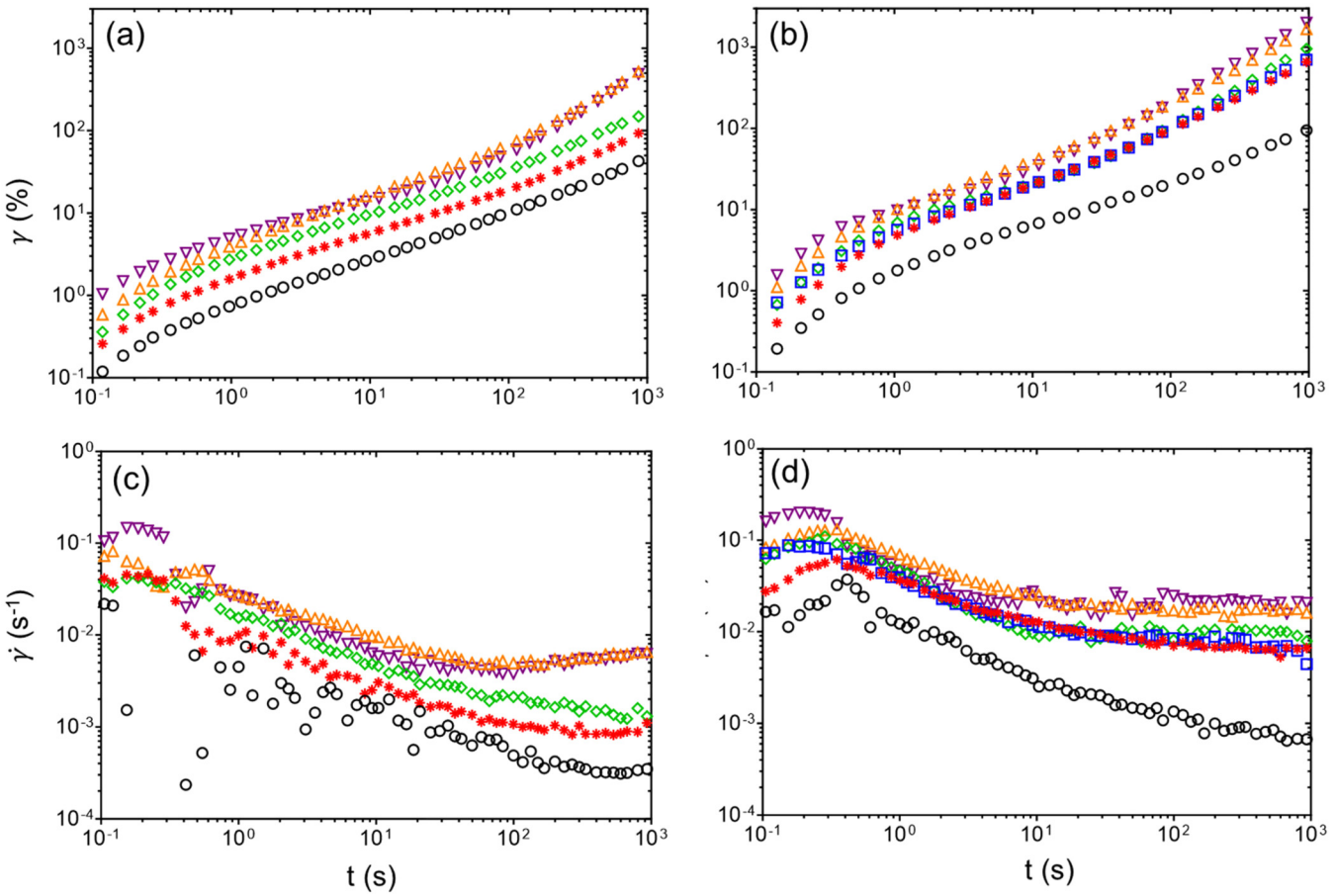

FIG. 7. (a) and (b) Strain deformation and (c) and (d) shear rate as a function of time during the creep experiment for suspensions of smooth [(a) and (c)] and rough colloids [(b) and (d)]. Applied stress during creep includes 0.01 Pa (black circle, ○), 0.02 Pa (red star, ∗), 0.03 Pa (blue squares, □), 0.035 Pa (green diamonds, ◇), 0.05 Pa (orange upward triangle △), and 0.07 Pa (purple downward triangle ▽).

are $\sigma_y^S = 0.025 \pm 0.013$ Pa, $\sigma_y^R = 0.015 \pm 0.005$ Pa, respectively.

Figure 9 shows that, despite small differences in the yield stress, suspensions of rough colloids exhibit a larger strain deformation at the end of the creep experiment ($t = 1000$ s, $\gamma = \gamma_{,max}$) as compared to suspensions of smooth colloids (average $\gamma_{R,max} = 96\%$, 670%, 968%, 1695%, 2039% and $\gamma_{S,max} = 47\%$, 106%, 166%, 596%, 560% for $\sigma a_{eff}^3/k_BT = 2.5$, 6.6, 11.7, 17, 24, respectively), irrespective of σ. Furthermore, for $0.03 \le \sigma \le 0.07$ Pa (i.e., $\sigma \ge \sigma_y$), rough colloids attain steady flow within 40–50 s while smooth colloids require 100–120 s. In other words, suspensions of rough

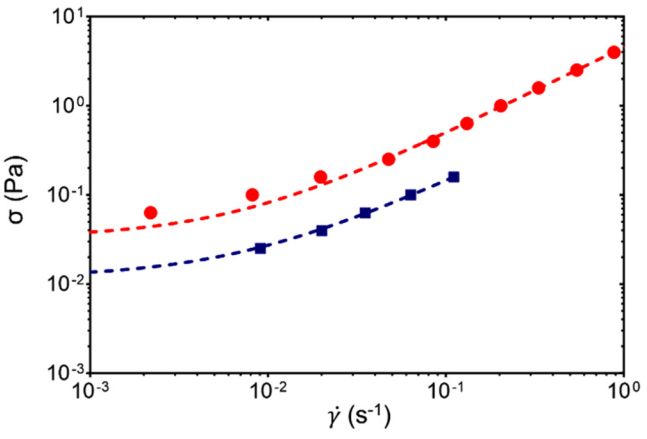

FIG. 8. Steady shear flow sweep showing applied stress as a function of the shear rate for suspensions of smooth (red circles) and rough colloids (blue squares) at a distance of 3.0% and 3.4%, for smooth and rough colloids, respectively, from jammed packing. The dotted lines represent Herschel–Bulkley fits to the flow curves.

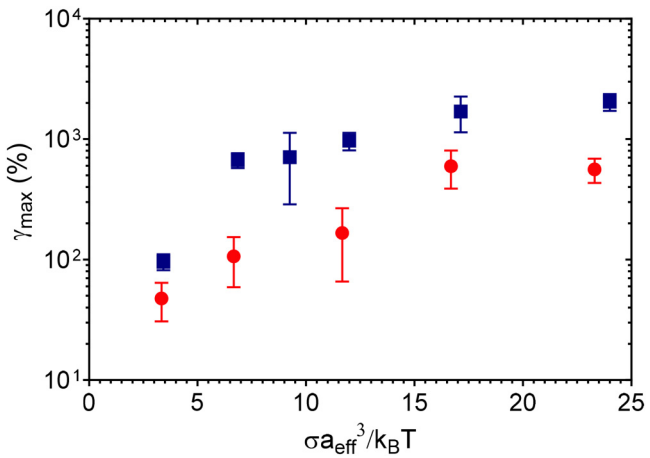

FIG. 9. Maximum strain deformation at the end of the creep experiment ($t = 1000$ s) as a function of applied stress scaled with respect to the particle size for suspensions of smooth (red circles) and rough (blue squares) colloids.

colloids fluidize more readily than smooth colloids. The higher strain deformation and earlier onset of fluidization in suspensions of rough colloids do not align with the expectation that rotational constraints imposed by the surface roughness might limit the strain deformation in creeping flow. The higher fluidization potential in creep flow is unlike that of the rheological properties found in $Pe > 100$ shear thickening flows, where rough colloids tend to exhibit stronger thickening responses because of rotational constraints and larger excluded volumes [27]. The higher creep strain of rough colloids could be due to a larger number of highly mobile particles. Sentjbrskaja *et al*. showed that the macroscopic creep deformation in hard-sphere colloidal glasses correlates linearly with the mean squared displacement and fraction of dynamically active particles, both above and below the yield stress [50]. Furthermore, the occurrence of steady flow coincides with the emergence of a region of higher local mobility that percolates throughout the sample at the yield stress, while dynamic activity remains localized below the yield stress. Similar results were obtained by Schall *et al*., who demonstrated that the number of shear transformation zones increases with increasing strain and that plastic flow occurs when such zones form a sample-spanning network [94]. Finally, Ghosh *et al*. also showed that sample fluidization in hard-sphere colloidal glasses was associated with the emergence of dynamical clusters of particles that percolated at the yielding transition [54]. Figures 7 and 9 suggest that interlocking particles, such as the rough colloids used in this study, could promote the formation of clusters with greater dynamical activity, perhaps due to the coordinated rotation of interlocked clusters. The enhanced cluster mobility results in a higher strain deformation and earlier onset of fluidization for rough colloids at a jamming distance that is equivalent to that of smooth colloids.

C. Recovery

When the stress is set to $\sigma = 0$ after the cessation of creep flow, the resultant strain recovery is a result of structural recovery and can be divided into recoverable (γ_{rec}) and nonrecoverable components (γ_{unrec}). The recoverable part of strain deformation is a measure of the remnant suspension elasticity, while the unrecoverable strain is associated with permanent deformation due to viscous losses [51,57,95]. The value of $\gamma_{rec}(t)$ is the difference between maximum strain deformation at the end of creep and the time-dependent strain measured during recovery [i.e., $\gamma_{rec}(t) = \gamma_{max} - \gamma_r(t)$]. The minimum changes in angular displacement (~100 nrad) measured in recovery experiments are far greater than the resolution (10 nrad) of the instrument, which ensures that the recoverable strain values reported here are reliable.

Figures 10(a) and 10(b) show the slow evolution of the γ_{rec} as a function of t. Irrespective of the previously applied creep stress, both types of suspensions only recover 10%–20% of the maximum recoverable strain ($\gamma_{rec,max}$, recoverable strain at the end of the recovery experiment $t = 3000$ s) within a short time frame of $t = 1$ s, while the majority of the recovery occurs gradually over the remaining period ($1 < t < 3000$ s). As mentioned in Sec. III B, the application of σ distorts the particle cages, causing particles above a reference particle to move in a different direction compared to the particles below the reference particle. The differential mobility builds up an internal anisotropic osmotic pressure, which drives recovery once the stress is removed [46]. Petekidis *et al*. reported that a major fraction (60%–80%) of $\gamma_{rec,max}$ in hard-sphere colloidal glasses is recovered at short times ($t \sim 1$ s), while the residual recovery occurs slowly over the remaining period of time [46,47]. They attributed the initial rapid recovery to the suspension elasticity and rapid β-relaxation of particle cages, indicative of the fast motion of particles within particle cages, while the residual recovery is attributed to the slow viscoelastic nature of the suspension and residual cage rearrangements [47]. It is likely that the absence of a distinct initial rapid recovery phase and long-term gradual recovery is due to the viscoelastic nature of our suspensions, with relatively equal contributions from both G' and G'', as opposed to the predominantly elastic colloidal glass reported in previous

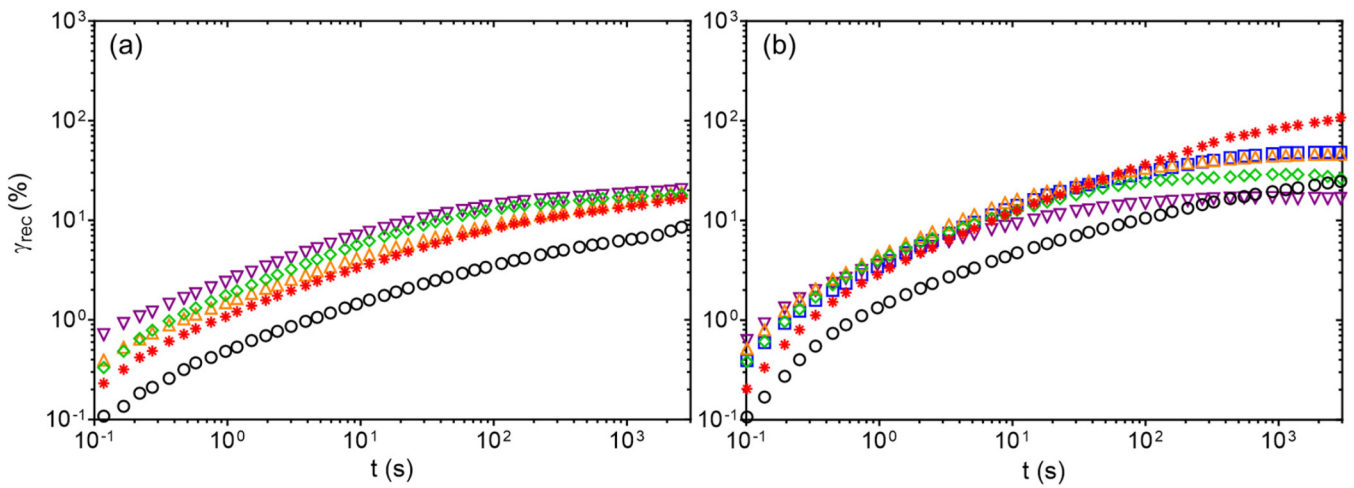

FIG. 10. Recoverable strain as a function of time during the recovery experiment for suspensions of (a) smooth and (b) rough colloids. Applied stress during creep includes 0.01 Pa (black circle, ○), 0.02 Pa (red star, ∗), 0.03 Pa (blue squares, □), 0.035 Pa (green diamonds, ◇), 0.05 Pa (orange upward triangle △), and 0.07 Pa (purple downward triangle ▽).

studies. This difference in the relative contribution of G' and G'' may arise because of the comparatively large particle size used in this study, in contrast with the submicrometer sized colloidal particles ($2a = 0.36$–$0.60\,\mu m$) used in previous studies [46,47,49].

Generally, for $\sigma < \sigma_y$, both $\gamma_{rec,max}$ and $\gamma_{rec,i}$ increase with σ since the suspension retains solidlike character, and the slope m (equivalent to $d\sigma/d\gamma_{rec,i}$) when plotting $\gamma_{rec,i}$ as a function of σ is equivalent to the value of G' obtained within the LVR [46,47]. For $\sigma > \sigma_y$, both $\gamma_{rec,max}$ and $\gamma_{rec,i}$ reach a saturation value (~10%–20%) independent of σ [49]. Some recovery is observed even after the suspensions achieve steady flow because particle dynamics during recovery are still affected by caging. As cages break and reform, out-of-cage particle motion remains restricted to a small distance corresponding to a fraction of the particle size (~10%–20%) [49]. The crossover between linearly increasing instantaneous recoverable strain ($\gamma_{rec,i}$) and its saturation value occurs at the suspension yield stress [46,47]. Figure 11 shows that $\gamma_{rec,i}$ ($t = 1$ s) for suspensions of rough colloids reaches a saturation value at 0.025 Pa, while suspensions of smooth colloids reach a saturated value at 0.035 Pa. These values are close to the yield stress values estimated from the steady shear flow sweep ($\sigma_y^S = 0.031$ Pa, $\sigma_y^R = 0.014$ Pa) and oscillatory stress sweep ($\sigma_y^S = \sigma_y^R = 0.010$ Pa). However, we observe that values of m ($m_S = 1.78$ Pa, $m_R = 0.64$ Pa) are greater than G' corresponding to the G' value obtained within the LVR regime during oscillatory stress sweep ($G'_S = 0.63$ Pa, $G'_R = 0.32$ Pa). We hypothesize that the deviation between the m and G' arises because both suspensions are only weakly elastic, which means that σ may not be directly proportional to $\gamma_{rec,i}$ even below σ_y. The weakly elastic nature of the suspensions is indicated by the loss modulus calculated based on G' and G'' obtained during the oscillatory stress sweep ($\tan\delta_S = \tan\delta_R \sim 1$).

We verify the hypothesis by running creep and recovery experiments on a suspension of submicrometer sized smooth colloidal particles ($2a = 0.73\,\mu m \pm 5\%$) at $\phi = 0.6$. Since G' is inversely proportional to the particle size ($G' \propto 1/a^3$), we expect suspensions with submicrometer sized colloidal particles to exhibit strongly elastic behavior within the linear regime. Figure 12 summarizes the results obtained from oscillatory stress sweep and creep and recovery experiments. As hypothesized, the slope of $\gamma_{rec,i}$ as a function of σ (5.1 Pa) for $\sigma < \sigma_y$ matches the G' value obtained within the linear regime of the oscillatory stress sweep (4.5 Pa). This agreement might be due to the strong solidlike elastic character ($\tan\delta_S = 0.45$) of the suspension of smaller colloids, which ensures a rapid solidlike recovery at short times and a gradual recovery at long times as reported in previous studies [46,47]. We chose $\phi = 0.6$ to obtain flowable suspensions for the experiments. The yield stress of the suspension, as indicated by a crossover of G' and G'', is 0.6 Pa. Therefore, after preshearing the loaded suspension, creep and recovery experiments were conducted between 0.01 and 5 Pa so that the strain responses both above and below the yield stress could be analyzed.

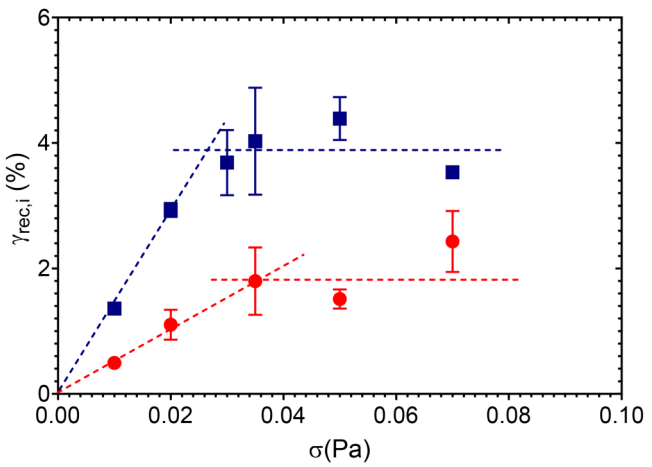

FIG. 11. Instantaneous recoverable strain ($t = 1$ s) as a function of applied stress for suspensions of smooth (red circles) and rough (blue squares) colloids during the recovery experiment. The dotted lines indicate linear fits below the yield stress and a saturation plateau beyond the yield stress.

Studies have shown that $\gamma_{rec,max}$ also exhibits an increase with σ for $\sigma < \sigma_y$ followed by saturation above σ_y in hard-sphere colloidal glasses [46,47]. Figure 13(a) shows that $\gamma_{rec,max}$ reaches a saturation value of (15%–18%) in suspensions of smooth colloids above 0.02 Pa. Unlike smooth colloids, Fig. 13(b) shows that suspensions of rough colloids exhibit a nonmonotonic trend in $\gamma_{rec,max}$ with a peak value of 100% at $\sigma = 0.02$ Pa ($\sim\sigma_y$) followed by decreasing $\gamma_{rec,max}$ with increasing σ. Such nonmonotonic behavior in γ_{rec} was reported by Pham *et al.* for attractive colloidal glasses [17,96]. Pham *et al.* observed that $\gamma_{rec,i}$ and $\gamma_{rec,max}$ increased with σ up to σ_y, followed by a decrease with increasing σ. They speculated that for $\sigma \ll \sigma_y$, interparticle attractive bonds respond elastically, preventing changes in the bonding and topological neighbors and leading to high recoverable strains up to σ_y. Beyond σ_y, flow-induced bond breaking competes with bond formation by diffusion and decreases the magnitude of $\gamma_{rec,max}$. For $\sigma \gg \sigma_y$, shear-driven bond breaking dominates, resulting in a value of $\gamma_{rex,max}$ with similar a magnitude as that of a hard-sphere colloidal glass. Analogous to attractive colloidal systems, the interlocking of surface asperities in jammed suspensions of rough colloids may function similarly to bonds formed from frictional interactions in particle cluster networks that can withstand applied shear and provide higher recovery up to 0.02 Pa. For $\sigma \leq 0.02$ Pa, the particle clusters might be stretched by applied shear without breaking the interlocking contacts so that upon removal of stress, the contacts exhibit greater elastic recovery compared to suspensions of smooth colloids. Beyond $\sigma = 0.02$ Pa, the applied shear begins to break the interlocking contacts, resulting in a decrease in γ_{rec} until it matches the recovery in suspensions of smooth colloids as observed at $\sigma = 0.07$ Pa.

It is important to note that while $\gamma_{rec,max}$ is higher for suspensions of rough colloids, Fig. 14 shows that, at similar σ, suspensions of smooth and rough colloids recover a similar fraction of the strain deformation accumulated during creep. The ratio of $\gamma_{rec,max}$ with respect to γ_{max} indicates the extent to which the suspension can recover the creep strain

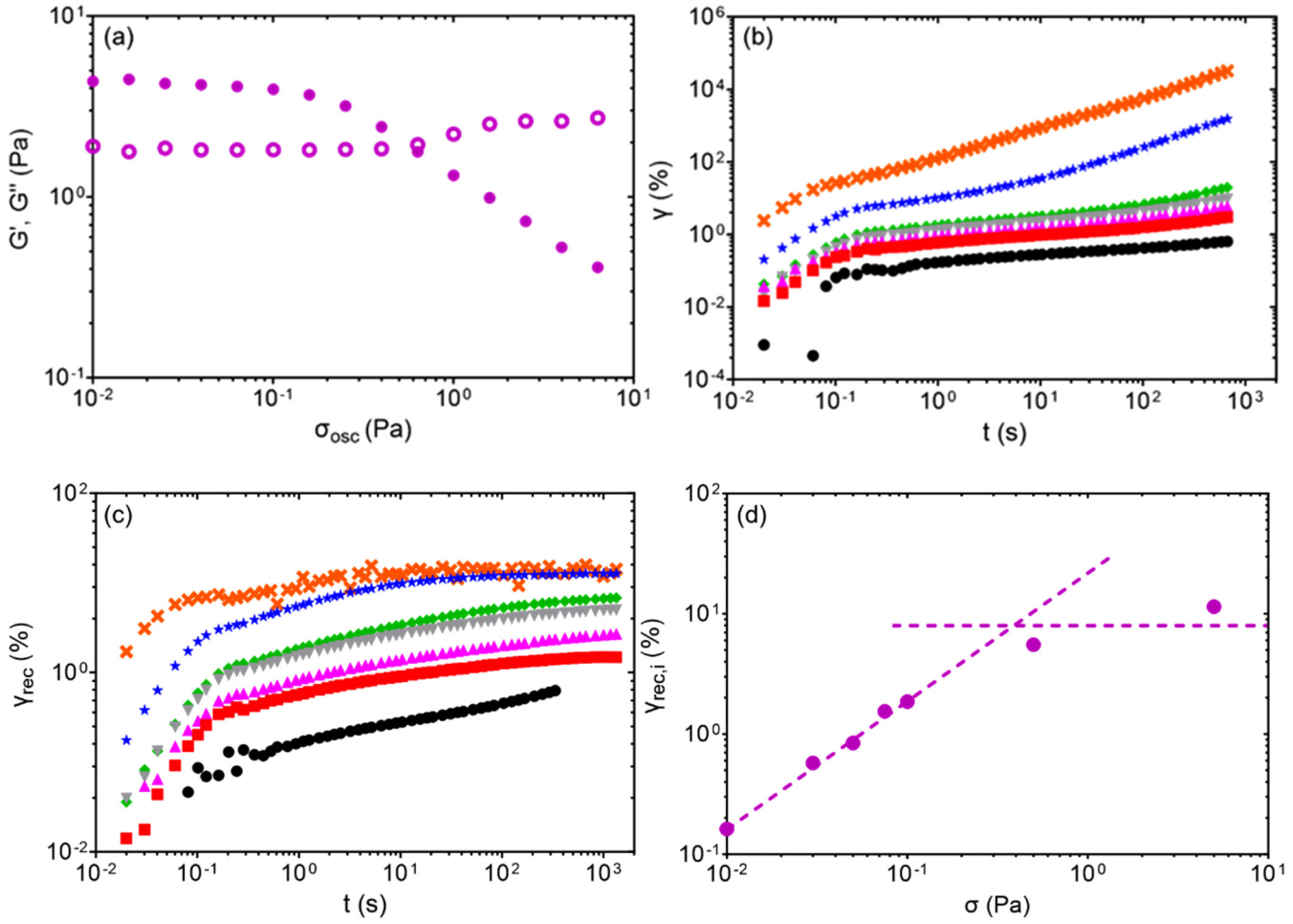

FIG. 12. (a) Oscillatory stress sweep performed on a suspension of smooth colloids of smaller sizes ($2a = 0.73\,\mu\text{m} \pm 5\%$, $f = 0.60$) showing the LVR, the onset of nonlinearity and crossover of G' (closed circles) and G'' (open circles). (b) Strain responses as a function of time and applied stress during creep. (c) Recoverable strain as a function of time and applied stress during recovery. (d) Instantaneous recoverable strain as a function of applied stress. Applied stress during creep include 0.01 Pa (black circle, ●), 0.05 Pa (red square, ■), 0.075 Pa (purple upward triangle, ▲), 0.1 Pa (gray downward triangle, ▼), 0.5 Pa (green diamond, ◆), 1 Pa (blue star, ★), and 5 Pa (orange cross, ✕).

deformation. As σ increases, the extent of recovery decreases for both systems, indicating greater permanent deformation. Even at the lowest applied stress of $\sigma = 0.01$ Pa, suspensions of smooth and rough colloids recover approximately 25% of strain deformation. This type of partial recovery has been previously reported for hard-sphere colloidal glasses and suggests that even below the yield stress, dense suspensions undergo permanent deformation due to viscous flow.

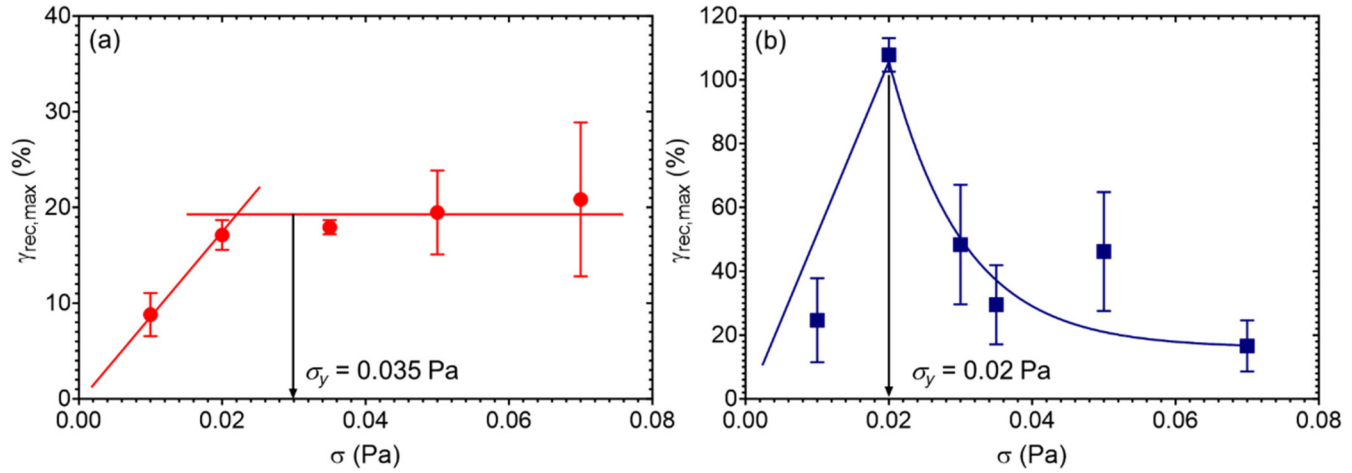

FIG. 13. Maximum recoverable strain at the end of the recovery experiment ($t = 3000$ s) as a function of applied stress for suspensions of smooth (left, red circles) and rough colloids (right, blue squares). Lines are drawn to guide the eye. Arrows indicate yield stresses for smooth and rough colloids obtained from creep experiments.

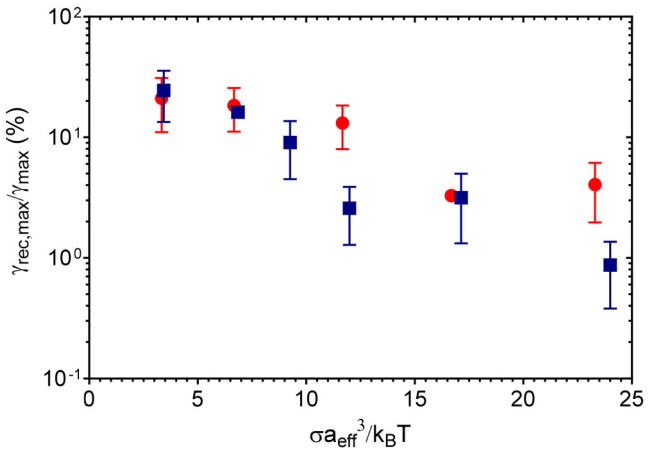

FIG. 14. Maximum fractional recovery at the end of the recovery experiment ($t = 3000$ s) as a function of applied stress scaled with respect to the particle size for suspensions of smooth (red circles) and rough (blue squares) colloids.

IV. CONCLUSIONS

This study combines oscillatory measurements, steady shear flow sweeps, as well as creep and recovery rheology to show how particle surface roughness affects the mechanical and flow properties of dense colloidal suspensions. At a jamming distance of 3.4% for smooth and rough colloids suspensions of rough colloids exhibit lower load-bearing capacity compared to suspensions of smooth colloids ($G_S' \sim 3G_R'$). Previous studies have shown that rough colloids experience hindered rotational dynamics due to interlocking of surface asperities at high concentrations [23,26]. The interlocking between immobile rough colloids may result in the formation of particle clusters that are not completely disrupted during shear rejuvenation, resulting in a weaker heterogeneous microstructure. Suspensions of smooth colloids may possess a homogeneous microstructure by avoiding cluster formation.

During creep, suspensions of rough colloids undergo higher strain deformation compared to smooth colloids both above and below σ_y and exhibit early onset of fluidization above σ_y. The magnitude of γ is likely correlated with the fraction of dynamically active particles, and the onset of fluidization occurs upon percolation of mobile particle clusters in hard-sphere colloidal glasses as described in this study and by others [50,54,94]. It is likely that, in addition to the weaker load-bearing capacity of rough colloids in creep flow, asperity interlocking facilitates percolation of active mobile clusters leading to greater dynamical activity for the same applied stress. Strain recovery experiments performed after creep show that $\gamma_{rec,max}$ increases nonmonotonically with respect to σ for suspensions of rough colloids. The value of $\gamma_{rec,max}$ (~100%) peaks at 0.02 Pa for suspensions of rough colloids, which matches the bulk yield stress obtained during creep ($\sigma_y^R = 0.02$ Pa), indicating a threshold below which particle interlocking results in long-lived contacts that can withstand the applied shear. However, for $\sigma > 0.02$ Pa, interlocked particle clusters begin to break, and at sufficiently high stress ($\sigma = 0.07$ Pa), suspensions of rough colloids exhibit similar $\gamma_{rec,max}$ as suspension of smooth colloids (15%–20%). Despite a higher magnitude of $\gamma_{rec,max}$ in rough colloids, the ratio of $\gamma_{rec,max}$ to γ_{max} shows that suspensions of smooth and rough colloids recover similar fractions of creep strain deformation. This indicates that both suspensions accumulate greater permanent strain deformation over time, irrespective of σ. Results from this study indicate that microscale particle properties, such as surface roughness, can significantly affect the flow and elastic recovery in dense suspensions and, therefore, serve as a design tool to generate novel yield stress fluids for applications such as additive manufacturing, coatings, and mechanically responsive soft matter composites.

ACKNOWLEDGMENTS

The authors thank Ronald Larson, George Petekidis, Dimitris Vlassopoulos, and Jeff Morris for scientific discussions. This work is supported by the International Fine Particles Research Institute (IFPRI, Grant No. 139A) and the National Science Foundation under Award Nos. CBET-1804462 and DMR-2104726.

AUTHOR DECLARATIONS

Conflict of Interest

The authors have no conflicts to disclose.

REFERENCES

[1] Bonn, D., M. M. Denn, L. Berthier, T. Divoux, and S. Manneville, "Yield stress materials in soft condensed matter," Rev. Mod. Phys. **89**(3), 035005 (2017).
[2] Ewoldt, R. H., and C. Saengow, "Designing complex fluids," Annu. Rev. Fluid Mech. **54**, 413–441 (2022).
[3] Leocmach, M., C. Perge, T. Divoux, and S. Manneville, "Creep and fracture of a protein gel under stress," Phys. Rev. Lett. **113**(3), 038303 (2014).
[4] Mariyate, J., and A. Bera, "Recent progresses of microemulsions-based nanofluids as a potential tool for enhanced oil recovery," Fuel **306**, 121640 (2021).
[5] Kramb, R., R. Zhang, K. S. Schweizer, and C. Zukoski, "Glass formation and shear elasticity in dense suspensions of repulsive anisotropic particles," Phys. Rev. Lett. **105**(5), 055702 (2010).
[6] Kramb, R. C., and C. F. Zukoski, "Nonlinear rheology and yielding in dense suspensions of hard anisotropic colloids," J. Rheol. **55**(5), 1069–1084 (2011).
[7] Townsend, J. M., E. C. Beck, S. H. Gehrke, C. J. Berkland, and M. S. Detamore, "Flow behavior prior to crosslinking: The need for precursor rheology for placement of hydrogels in medical applications and for 3D bioprinting," Prog. Polym. Sci. **91**, 126–140 (2019).
[8] Nelson, A. Z., K. S. Schweizer, B. M. Rauzan, R. G. Nuzzo, J. Vermant, and R. H. Ewoldt, "Designing and transforming yield-stress fluids," Curr. Opin. Solid State Mater. Sci. **23**(5), 100758 (2019).
[9] Eshgarf, H., A. A. Nadooshan, and A. Raisi, "An overview on properties and applications of magnetorheological fluids: Dampers, batteries, valves and brakes," J. Energy Storage **50**, 104648 (2022).
[10] Ewoldt, R. H., "Extremely soft: Design with rheologically complex fluids," Soft Robot. **1**(1), 12–20 (2014).
[11] Nelson, A. Z., R. E. Bras, J. Liu, and R. H. Ewoldt, "Extending yield-stress fluid paradigms," J. Rheol. **62**(1), 357–369 (2018).

[12] Christopoulou, C., G. Petekidis, B. Erwin, M. Cloitre, and D. Vlassopoulos, "Ageing and yield behaviour in model soft colloidal glasses," Philos. Trans. R. Soc. Math. Phys. Eng. Sci. **367**(1909), 5051–5071 (2009).

[13] Le Grand, A., and G. Petekidis, "Effects of particle softness on the rheology and yielding of colloidal glasses," Rheol. Acta **47**, 579–590 (2008).

[14] Kramb, R. C., and C. F. Zukoski, "Yielding in dense suspensions: Cage, bond, and rotational confinements," J. Phys.: Condens. Matter **23**(3), 035102 (2010).

[15] Sentjabrskaja, T., E. Babaliari, J. Hendricks, M. Laurati, G. Petekidis, and S. U. Egelhaaf, "Yielding of binary colloidal glasses," Soft Matter **9**(17), 4524–4533 (2013).

[16] Sentjabrskaja, T., J. Hendricks, A. R. Jacob, G. Petekidis, S. U. Egelhaaf, and M. Laurati, "Binary colloidal glasses under transient stress-and strain-controlled shear," J. Rheol. **62**(1), 149–159 (2018).

[17] Pham, K. N., G. Petekidis, D. Vlassopoulos, S. U. Egelhaaf, W. C. K. Poon, and P. N. Pusey, "Yielding behavior of repulsion-and attraction-dominated colloidal glasses," J. Rheol. **52**(2), 649–676 (2008).

[18] Zaccarelli, E., and W. C. K. Poon, "Colloidal glasses and gels: The interplay of bonding and caging," Proc. Natl. Acad. Sci. U.S.A. **106**(36), 15203–15208 (2009).

[19] Chan, H. K., and A. Mohraz, "Microdynamics of dense colloidal suspensions and gels under constant-stress deformation," J. Rheol. **58**(5), 1419–1439 (2014).

[20] Reddy, G. R. K., and Y. M. Joshi, "Aging under stress and mechanical fragility of soft solids of laponite," J. Appl. Phys. **104**(9), 094901 (2008).

[21] Richards, J., B. Guy, E. Blanco, M. Hermes, G. Poy, and W. Poon, "The role of friction in the yielding of adhesive non-Brownian suspensions," J. Rheol. **64**(2), 405–412 (2020).

[22] Guy, B., J. Richards, D. Hodgson, E. Blanco, and W. Poon, "Constraint-based approach to granular dispersion rheology," Phys. Rev. Lett. **121**(12), 128001 (2018).

[23] Hsiao, L. C., I. Saha-Dalal, R. G. Larson, and M. J. Solomon, "Translational and rotational dynamics in dense suspensions of smooth and rough colloids," Soft Matter **13**(48), 9229–9236 (2017).

[24] Pradeep, S., A. Wessel, and L. C. Hsiao, "Hydrodynamic origin for the suspension viscoelasticity of rough colloids," J. Rheol. **66**(5), 895–906 (2022).

[25] Schroyen, B., C.-P. Hsu, L. Isa, P. Van Puyvelde, and J. Vermant, "Stress contributions in colloidal suspensions: The smooth, the rough, and the hairy," Phys. Rev. Lett. **122**(21), 218001 (2019).

[26] Ilhan, B., F. Mugele, and M. H. G. Duits, "Roughness induced rotational slowdown near the colloidal glass transition," J. Colloid Interface Sci. **607**, 1709–1716 (2022).

[27] Pradeep, S., M. Nabizadeh, A. R. Jacob, S. Jamali, and L. C. Hsiao, "Jamming distance dictates colloidal shear thickening," Phys. Rev. Lett. **127**(15), 158002 (2021).

[28] Hsu, C.-P., S. N. Ramakrishna, M. Zanini, N. D. Spencer, and L. Isa, "Roughness-dependent tribology effects on discontinuous shear thickening," Proc. Natl. Acad. Sci. U.S.A. **115**(20), 5117–5122 (2018).

[29] Lootens, D., H. Van Damme, Y. Hémar, and P. Hébraud, "Dilatant flow of concentrated suspensions of rough particles," Phys. Rev. Lett. **95**(26), 268302 (2005).

[30] Royer, J. R., D. L. Blair, and S. D. Hudson, "Rheological signature of frictional interactions in shear thickening suspensions," Phys. Rev. Lett. **116**(18), 188301 (2016).

[31] Hsiao, L. C., S. Jamali, E. Glynos, P. F. Green, R. G. Larson, and M. J. Solomon, "Rheological state diagrams for rough colloids in shear flow," Phys. Rev. Lett. **119**(15), 158001 (2017).

[32] Bourrianne, P., V. Niggel, G. Polly, T. Divoux, and G. H. McKinley, "Tuning the shear thickening of suspensions through surface roughness and physico-chemical interactions," Phys. Rev. Res. **4**(3), 033062 (2022).

[33] San-Miguel, A., and S. H. Behrens, "Influence of nanoscale particle roughness on the stability of pickering emulsions," Langmuir **28**(33), 12038–12043 (2012).

[34] Zanini, M., C. Marschelke, S. E. Anachkov, E. Marini, A. Synytska, and L. Isa, "Universal emulsion stabilization from the arrested adsorption of rough particles at liquid-liquid interfaces," Nat. Commun. **8**(1), 15701 (2017).

[35] Zanini, M., A. Cingolani, C.-P. Hsu, MÁ Fernández-Rodríguez, G. Soligno, A. Beltzung, S. Caimi, D. Mitrano, G. Storti, and L. Isa, "Mechanical phase inversion of pickering emulsions via metastable wetting of rough colloids," Soft Matter **15**(39), 7888–7900 (2019).

[36] Weijgertze, H. M., W. K. Kegel, and M. Zanini, "Patchy rough colloids as pickering stabilizers," Soft Matter **16**(34), 8002–8012 (2020).

[37] Hermes, M., and P. S. Clegg, "Yielding and flow of concentrated pickering emulsions," Soft Matter **9**(31), 7568–7575 (2013).

[38] Hsu, C.-P., H. E. Baysal, G. Wirenborn, G. Mårtensson, L. P. Wittberg, and L. Isa, "Roughness-dependent clogging of particle suspensions flowing into a constriction," Soft Matter **17**(31), 7252–7259 (2021).

[39] Rice, R., R. Roth, and C. P. Royall, "Polyhedral colloidal 'rocks': Low-dimensional networks," Soft Matter **8**(4), 1163–1167 (2012).

[40] Weeks, E. R., "Introduction to the colloidal glass transition," ACS Macro Lett. **6**(1), 27–34 (2017).

[41] Weeks, E. R., and D. Weitz, "Properties of cage rearrangements observed near the colloidal glass transition," Phys. Rev. Lett. **89**(9), 095704 (2002).

[42] Weeks, E. R., and D. A. Weitz, "Subdiffusion and the cage effect studied near the colloidal glass transition," Chem. Phys. **284**(1–2), 361–367 (2002).

[43] Weeks, E. R., J. C. Crocker, A. C. Levitt, A. Schofield, and D. A. Weitz, "Three-dimensional direct imaging of structural relaxation near the colloidal glass transition," Science **287**(5453), 627–631 (2000).

[44] Hunter, G. L., and E. R. Weeks, "The physics of the colloidal glass transition," Rep. Prog. Phys. **75**(6), 066501 (2012).

[45] Petekidis, G., A. Moussaid, and P. Pusey, "Rearrangements in hard-sphere glasses under oscillatory shear strain," Phys. Rev. E **66**(5), 051402 (2002).

[46] Petekidis, G., D. Vlassopoulos, and P. N. Pusey, "Yielding and flow of sheared colloidal glasses," J. Phys.: Condens. Matter **16**(38), S3955–S3963 (2004).

[47] Petekidis, G., D. Vlassopoulos, and P. N. Pusey, "Yielding and flow of colloidal glasses," Faraday Discuss. **123**, 287–302 (2003).

[48] Ballesta, P., and G. Petekidis, "Creep and aging of hard-sphere glasses under constant stress," Phys. Rev. E **93**(4), 042613 (2016).

[49] Pamvouxoglou, A., A. B. Schofield, G. Petekidis, and S. U. Egelhaaf, "Stress versus strain controlled shear: Yielding and relaxation of concentrated colloidal suspensions," J. Rheol. **65**(6), 1219–1233 (2021).

[50] Sentjabrskaja, T., P. Chaudhuri, M. Hermes, W. C. K. Poon, J. Horbach, S. U. Egelhaaf, and M. Laurati, "Creep and flow of glasses: Strain response linked to the spatial distribution of dynamical heterogeneities," Sci. Rep. **5**(1), 1–11 (2015).

[51] Donley, G. J., S. Narayanan, M. A. Wade, J. D. Park, R. L. Leheny, J. L. Harden, and S. A. Rogers, "Investigation of the yielding transition in concentrated colloidal systems via rheo-XPCS," Proc. Natl. Acad. Sci. U.S.A. **120**(18), e2215517120 (2023).

[52] Siebenbürger, M., M. Ballauff, and T. Voigtmann, "Creep in colloidal glasses," Phys. Rev. Lett. **108**(25), 255701 (2012).

[53] Popovic, M., T. W. de Geus, W. Ji, A. Rosso, and M. Wyart, "Scaling description of creep flow in amorphous solids," Phys. Rev. Lett. **129**(20), 208001 (2022).

[54] Ghosh, A., Z. Budrikis, V. Chikkadi, A. L. Sellerio, S. Zapperi, and P. Schall, "Direct observation of percolation in the yielding transition of colloidal glasses," Phys. Rev. Lett. **118**(14), 148001 (2017).
[55] Laurati, M., P. Maßhoff, K. J. Mutch, S. U. Egelhaaf, and A. Zaccone, "Long-lived neighbors determine the rheological response of glasses," Phys. Rev. Lett. **118**(1), 018002 (2017).
[56] Sentjabrskaja, T., M. Hermes, W. Poon, C. Estrada, R. Castaneda-Priego, S. Egelhaaf, and M. Laurati, "Transient dynamics during stress overshoots in binary colloidal glasses," Soft Matter **10**(34), 6546–6555 (2014).
[57] Donley, G. J., P. K. Singh, A. Shetty, and S. A. Rogers, "Elucidating the G ″overshoot in soft materials with a yield transition via a time-resolved experimental strain decomposition," Proc. Natl. Acad. Sci. U.S.A. **117**(36), 21945–21952 (2020).
[58] Denisov, D. V., M. T. Dang, B. Struth, A. Zaccone, G. H. Wegdam, and P. Schall, "Sharp symmetry-change marks the mechanical failure transition of glasses," Sci. Rep. **5**(1), 14359 (2015).
[59] Dang, M. T., D. Denisov, B. Struth, A. Zaccone, and P. Schall, "Reversibility and hysteresis of the sharp yielding transition of a colloidal glass under oscillatory shear," Eur. Phys. J. E **39**, 44 (2016).
[60] Furst, E. M., "Applications of laser tweezers in complex fluid rheology," Curr. Opin. Colloid Interface Sci. **10**(1–2), 79–86 (2005).
[61] Amann, C. P., D. Denisov, M. T. Dang, B. Struth, P. Schall, and M. Fuchs, "Shear-induced breaking of cages in colloidal glasses: Scattering experiments and mode coupling theory," J. Chem. Phys. **143**(3), 034505 (2015).
[62] Van Megen, W., and S. Underwood, "Glass transition in colloidal hard spheres: Mode-coupling theory analysis," Phys. Rev. Lett. **70**(18), 2766–2769 (1993).
[63] Van Megen, W., and S. Underwood, "Glass transition in colloidal hard spheres: Measurement and mode-coupling-theory analysis of the coherent intermediate scattering function," Phys. Rev. E **49**(5), 4206–4220 (1994).
[64] Schweizer, K. S., and E. J. Saltzman, "Activated hopping, barrier fluctuations, and heterogeneity in glassy suspensions and liquids," J. Phys. Chem. B **108**(51), 19729–19741 (2004).
[65] Ghosh, A., and K. S. Schweizer, "Microscopic activated dynamics theory of the shear rheology and stress overshoot in ultradense glass-forming fluids and colloidal suspensions," J. Rheol. **67**(2), 559–578 (2023).
[66] Ghosh, A., and K. S. Schweizer, "The role of collective elasticity on activated structural relaxation, yielding, and steady state flow in hard sphere fluids and colloidal suspensions under strong deformation," J. Chem. Phys. **153**(19), 194502 (2020).
[67] Yatsenko, G., and K. S. Schweizer, "Ideal glass transitions, shear modulus, activated dynamics, and yielding in fluids of nonspherical objects," J. Chem. Phys. **126**(1), 014505 (2007).
[68] Zhang, R., and K. S. Schweizer, "Theory of coupled translational-rotational glassy dynamics in dense fluids of uniaxial particles," Phys. Rev. E **80**(1), 011502 (2009).
[69] Moghimi, E., and G. Petekidis, "Mechanisms of two-step yielding in attractive colloidal glasses," J. Rheol. **64**(5), 1209–1225 (2020).
[70] Koumakis, N., and G. Petekidis, "Two step yielding in attractive colloids: Transition from gels to attractive glasses," Soft Matter **7**(6), 2456–2470 (2011).
[71] Pradeep, S., and L. C. Hsiao, "Contact criterion for suspensions of smooth and rough colloids," Soft Matter **16**(21), 4980–4989 (2020).
[72] Farr, R. S., and R. D. Groot, "Close packing density of polydisperse hard spheres," J. Chem. Phys. **131**(24), 244104 (2009).
[73] Phan, S.-E., W. B. Russel, J. Zhu, and P. M. Chaikin, "Effects of polydispersity on hard sphere crystals," J. Chem. Phys. **108**(23), 9789–9795 (1998).
[74] Schaertl, W., and H. Sillescu, "Brownian dynamics of polydisperse colloidal hard spheres: Equilibrium structures and random close packings," J. Stat. Phys. **77**(5), 1007–1025 (1994).
[75] Percus, J. K., and G. J. Yevick, "Analysis of classical statistical mechanics by means of collective coordinates," Phys. Rev. **110**(1), 1–13 (1958).
[76] Eilers, v. H., "Die viskosität von emulsionen hochviskoser stoffe als funktion der konzentration," Kolloid Z. **97**(3), 313–321 (1941).
[77] Abbasi Moud, A., J. Poisson, Z. M. Hudson, and S. G. Hatzikiriakos, "Yield stress and wall slip of kaolinite networks," Phys. Fluids **33**(5), 053105 (2021).
[78] Ballesta, P., G. Petekidis, L. Isa, W. C. K. Poon, and R. Besseling, "Wall slip and flow of concentrated hard-sphere colloidal suspensions," J. Rheol. **56**(5), 1005–1037 (2012).
[79] Buscall, R., "Wall slip in dispersion rheometry," J. Rheol. **54**(6), 1177–1183 (2010).
[80] Cloitre, M., and R. T. Bonnecaze, "A review on wall slip in high solid dispersions," Rheol. Acta **56**, 283–305 (2017).
[81] Paredes, J., N. Shahidzadeh, and D. Bonn, "Wall slip and fluidity in emulsion flow," Phys. Rev. E **92**(4), 042313 (2015).
[82] Yoshimura, A., and R. K. Prud'homme, "Wall slip corrections for Couette and parallel disk viscometers," J. Rheol. **32**(1), 53–67 (1988).
[83] Lee, J., Z. Jiang, J. Wang, A. R. Sandy, S. Narayanan, and X.-M. Lin, "Unraveling the role of order-to-disorder transition in shear thickening suspensions," Phys. Rev. Lett. **120**(2), 028002 (2018).
[84] Joshi, Y. M., "Dynamics of colloidal glasses and gels," Annu. Rev. Chem. Biomol. Eng. **5**, 181–202 (2014).
[85] Joshi, Y. M., and G. Petekidis, "Yield stress fluids and ageing," Rheol. Acta **57**, 521–549 (2018).
[86] Conrad, J. C., P. P. Dhillon, E. R. Weeks, D. R. Reichman, and D. A. Weitz, "Contribution of slow clusters to the bulk elasticity near the colloidal glass transition," Phys. Rev. Lett. **97**(26), 265701 (2006).
[87] Moghimi, E., A. R. Jacob, N. Koumakis, and G. Petekidis, "Colloidal gels tuned by oscillatory shear," Soft Matter **13**(12), 2371–2383 (2017).
[88] Mewis, J., and N. J. Wagner, *Colloidal Suspension Rheology* (Cambridge University, New York, 2012).
[89] Phillips, R., J. Brady, and G. Bossis, "Hydrodynamic transport properties of hard-sphere dispersions. I.: Suspensions of freely mobile particles," Phys. Fluids **31**(12), 3462–3472 (1988).
[90] Miguel, M.-C., A. Vespignani, M. Zaiser, and S. Zapperi, "Dislocation jamming and Andrade creep," Phys. Rev. Lett. **89**(16), 165501 (2002).
[91] Divoux, T., C. Barentin, and S. Manneville, "From stress-induced fluidization processes to Herschel-Bulkley behaviour in simple yield stress fluids," Soft Matter **7**(18), 8409–8418 (2011).
[92] Andrade, E. N. D. C., "On the viscous flow in metals, and allied phenomena," Proc. R. Soc. Lond. Ser., A **84**(567), 1–12 (1910).
[93] Ewoldt, R. H., and G. H. McKinley, "Creep ringing in rheometry or how to deal with oft-discarded data in step stress tests!," Rheol. Bull. **76**(4), 4–6, 22–24 (2007).
[94] Schall, P., D. A. Weitz, and F. Spaepen, "Structural rearrangements that govern flow in colloidal glasses," Science **318**(5858), 1895–1899 (2007).
[95] Singh, P. K., J. C.-W. Lee, K. A. Patankar, and S. A. Rogers, "Revisiting the basis of transient rheological material functions: Insights from recoverable strain measurements," J. Rheol. **65**(2), 129–144 (2021).
[96] Pham, K., G. Petekidis, D. Vlassopoulos, S. Egelhaaf, P. Pusey, and W. Poon, "Yielding of colloidal glasses," Europhys. Lett. **75**(4), 624–630 (2006).